

The effect of surfactant-free TiO₂ surface hydroxyl groups on physicochemical, optical and self-cleaning properties of developed coatings on polycarbonate

This content has been downloaded from IOPscience. Please scroll down to see the full text.

2013 J. Phys. D: Appl. Phys. 46 505316

(<http://iopscience.iop.org/0022-3727/46/50/505316>)

View [the table of contents for this issue](#), or go to the [journal homepage](#) for more

Download details:

IP Address: 131.247.208.144

This content was downloaded on 24/05/2014 at 19:58

Please note that [terms and conditions apply](#).

The effect of surfactant-free TiO₂ surface hydroxyl groups on physicochemical, optical and self-cleaning properties of developed coatings on polycarbonate

H Yaghoubi¹, A Dayerizadeh¹, S Han, M Mulaj³, W Gao², X Li²,
M Muschol³, S Ma² and A Takshi¹

¹ Bio/Organic Electronics Lab, Department of Electrical Engineering, University of South Florida, Tampa, FL 33620, USA

² Department of Chemistry, University of South Florida, Tampa, FL 33620, USA

³ Department of Physics, University of South Florida, Tampa, FL 33620, USA

E-mail: hyaghoubi@mail.usf.edu and Yaghoubi.houman@gmail.com

Received 26 August 2013, in final form 13 October 2013


Published 27 November 2013

Online at stacks.iop.org/JPhysD/46/505316

Abstract

TiO₂ is a prototypical transition metal oxide with physicochemical properties that can be modified more readily through sol–gel synthesis than through other techniques. Herein, we report on the change in the density of the hydroxyl groups on the surface of synthesized surfactant-free TiO₂ nanoparticles in water due to varying the pH (7.3, 8.3, 9.3 and 10.3) of the peroxotitanium complex, i.e. the amorphous sol, prior to refluxing. This resulted in colloidal solutions with differing crystallinity, nanoparticle size, optical indirect bandgaps and photocatalytic activity. It was shown that increasing the density of hydroxyl groups on TiO₂ particles coupled with low-temperature annealing (90 °C) induced an anatase to rutile transformation. Increasing the pH of the peroxotitanium complex interrupted the formation of anatase phase in crystalline sol, as evidenced by intensity increases of the Raman bands at ~822 (Ti–O–H) and 906 cm⁻¹ (vibrational Ti–O–H) and an intensity decrease of the band at 150 cm⁻¹ (anatase photonic E_g). Films prepared from higher pH suspensions showed lower roughness. The reaction rate constants for photo-induced self-cleaning activity of TiO₂ films prepared from colloidal solutions at pH 7.3, 8.3, 9.3 and 10.3 were estimated at 0.017 s⁻¹, 0.014 s⁻¹, 0.007 s⁻¹ and 0.006 s⁻¹, respectively.

(Some figures may appear in colour only in the online journal)

 Online supplementary data available from stacks.iop.org/JPhysD/46/505316/mmedia

1. Introduction

TiO₂ is one of the most promising candidate materials for environmentally friendly renewable energy applications due to its tailored photoactivity, photo and chemical stability, non-toxicity, low cost, and favourable redox potential [1–5]. Since the discovery of the Honda–Fujishima effect of TiO₂ in 1967 for applications in photoelectrochemical water splitting [1], research has revealed other characteristics and applications of this wide bandgap semiconductor, e.g. CO₂ reduction

to produce carbonaceous solar fuels, decontamination, water purification, hydrophilicity under UV irradiation, and self-cleansing [5–8]. The self-cleaning mechanism is mainly based on TiO₂ photocatalysis, where photo-induced electron–holes catalyse reaction on the surface [6, 7, 9]. The design of different forms of TiO₂ with various levels of dimensionality has also been investigated and reviewed thoroughly [10, 11].

As two-dimensional self-cleaning material, TiO₂ coatings may find numerous applications in the renewable energy field, such as on photovoltaic panels, for which dust and

contaminants are primary efficiency drains [5]. A recent review summarizes the key areas of self-cleaning coatings [12]. These coatings can be prepared on different substrate materials including glass [13, 14], construction materials [15, 16], fabrics [17–20], and polymers [9, 21, 22]. Lightweight self-cleaning materials are particularly appealing, both for environmental and cost considerations [5]. TiO₂ thin films applied on polymers have also shown a higher rate of photocatalytic activity than those on glass [9, 23–25]. In particular, polycarbonate (PC) has many advantages over glass, e.g. applications in earthquake prone areas as windows in skyscrapers in lieu of glass as well as in the auto industry for headlight enclosures. Yaghoubi recently comprehensively reviewed the existing knowledge of TiO₂ self-cleaning nanostructured materials on polymers [5].

The physicochemical properties of TiO₂ can largely affect its self-cleaning behaviour. The self-cleaning activity of TiO₂ mainly relates to three properties: morphology, crystal phase, and light-use efficiency. Compared to other techniques, these properties can be modified more readily through the sol–gel synthesis. Sol–gel synthesis is also considered as a facile preparation technique for low-temperature development of TiO₂ on low thermal resistance material, e.g. polymers [17]. In TiO₂ sol–gel synthesis the change in the density of hydroxyl groups on the TiO₂ particles can change the rates of hydrolysis and polycondensation of the titanium alkoxide, which induce physicochemical and structural alterations. Electrochemical experiments have confirmed the importance of hydroxyl groups in promoting electron transfer (ET) from the conduction band of TiO₂ to chemisorbed oxygen molecules [26]. The pH of the reaction medium can be varied to change the density of hydroxyl groups on the surface of TiO₂ particles. Herein, we employ confocal Raman spectroscopy to display the increase of TiO₂ surface hydroxyl groups and its effect on the phase transformation with increasing pH. Other techniques i.e. UV–Vis spectroscopy, dynamic light scattering (DLS), x-ray diffraction (XRD), atomic force microscopy (AFM), and photocatalytic tests have been employed here to probe the effect of surface-bound hydroxyl groups on physicochemical properties of TiO₂.

Raman scattering as a local probe is sensitive to the crystallinity and microstructure of materials [27]. The phonon confinement effects in the Raman scattering by TiO₂ nanocrystals have been previously studied [28, 29]. Nevertheless, the majority of the investigations to date have focused on the phonon confinement effects on the strongest $\sim 144\text{ cm}^{-1}$ anatase photonic E_g phonon. There has been little analysis of the phonon of other symmetries, except for a recent work by Sahoo *et al* [30].

An advanced understanding of the parameters that determine crystallinity and phase formation is crucial for the successful technological application of TiO₂ self-cleaning nanomaterials. TiO₂ surface chemical properties affect the flat band potential (i.e. the potential that needs to be applied to a semiconductor to eliminate the space charge layer) and, consequently, the charge transfer from the photocatalyst to the adsorbate [31]. This change in the flat band potential in turn affects the photocatalytic activity of TiO₂. The

previous studies have mainly investigated the effects of pH on crystallinity and particle size in the acidic range, i.e. $\text{pH} \leq 7$ [32, 33]. Others have investigated the effect of –OH– groups adsorbed from the atmosphere on the TiO₂ films by increasing the humidity [34]. In this work, we synthesize surfactant-free TiO₂ nanoparticles in water using the peroxotitanium complex as a starting material. By varying the surface acidity ($10.3 \geq \text{pH} \geq 7.3$) of TiO₂ particles, we determine the influence of the reactant chemistry, on the formation of the crystalline phase-mixed TiO₂ oxide systems. By doing this, one of our main objectives is to gain insight into the phase formation mechanisms through the density of hydroxylated groups on the TiO₂ particles (not in the solvent). In addition, we want to gain an in-depth understanding of how varying the pH of TiO₂ colloidal amorphous solutions can affect the physicochemical, optical, and self-cleaning properties of TiO₂ crystalline sols as well as developed coatings on PC substrates.

2. Experimental

2.1. Materials and synthesis

1 mm thick PC sheets were purchased from Bayer Corp., Germany. Potassium dichromate (Cr₂K₂O₇), 95–98% sulfuric acid (H₂SO₄), and titanium (IV) isopropoxide (TTIP) were purchased from Sigma-Aldrich. 30% hydrogen peroxide (H₂O₂) was purchased from J.T. Baker. Methylene blue hydrate (MB) was purchased from Fluka-Analytical. The PC substrates were cut into 25 mm × 20 mm pieces, cleaned, and chemically treated by immersing in a mixture of H₂SO₄ and Cr₂K₂O₇ as explained earlier [9]. Amorphous solutions of TiO₂ were prepared as explained in our earlier work [9, 13]. Briefly, a peroxotitanium complex solution was prepared by mixing TTIP, H₂O₂ and H₂O with volume proportions of 12 : 90 : 200, respectively. The resulting amorphous solution was then divided into four batches. NH₄OH was used to adjust the pH of the four batches with corresponding pH levels of 7.3, 8.3, 9.3 and 10.3, respectively. It is essential to note that all pH adjustments and measurements were performed on the amorphous sol, i.e. the peroxotitanium complex, prior to being refluxed for 10 h to obtain the crystalline phase. All references to pH levels in this study refer to measurements performed in the amorphous state. TiO₂ layers were spin-coated onto PC substrates at 1000 rpm for 1 min following this procedure: for all the samples, a pre-coat of the peroxotitanium complex was applied initially on the surface of PC substrates. This first layer was then dried in a vacuum furnace at 90 °C for 15 min. Four subsequent layers of crystalline TiO₂ were applied over the amorphous layer following the same procedure. Finally, the samples were annealed in vacuum at 90 °C for 1 h.

2.2. Characterization

Optical absorption and transmission of TiO₂ colloidal solutions and thin films at different pH levels was determined using a Thermo Scientific (Evolution 201) UV–Vis spectrophotometer. The optical indirect band gap energies of TiO₂ sols at different pH levels were also determined from the absorbance spectra. It is essential to note that all the bandgap measurements in

this work refer to optical indirect energy of the bandgap, estimated from absorption spectrum, which is different from electronic bandgap (which can be measure by x-ray, ultraviolet and inverse photoemission spectroscopy). The hydrodynamic radius of TiO₂ nanoparticles in the aqueous sol was measured using DLS (Malvern, Zetasizer Nano S with 633 nm HeNe laser) at room temperature (25 °C) and with the original sol being diluted by a factor of fifty in order to ensure colloidal stability and to minimize scattering. All the Raman experiments were carried out using a confocal Raman microscope from Horiba Jovin Yvon, equipped with an Argon and Krypton laser (Coherent, Innova 70 C series). An excitation laser wavelength at 514 nm was used with a power of 78 mW at room temperature. Three accumulations and 5 s exposure times were employed for all the samples. The spectrograph grating was 600 grooves mm⁻¹ and a 20× objective was used. Raman spectra ranging from 50 to 4000 cm⁻¹ were collected. However, only the region with interesting peaks from 100 to 1000 cm⁻¹ is shown and discussed here. To show the role of hydroxyl groups on the TiO₂ nanoparticles, the Raman spectra of the solvent was obtained by isolating it from the nanoparticles using an electrophoresis technique. An apparatus using a working (anode) and a counter (cathode) electrode of stainless steel was set up. The electrodes were placed vertically in a 25 ml beaker containing the crystalline TiO₂ nanoparticle solutions. The distance between the two electrodes and the surface of the electrodes was 1.5 cm and 4.5 cm, respectively. The electrophoretic deposition was carried out by applying 5 V across the cell. The voltage was increased gradually up to ~13 V, until the solvent (water) and the TiO₂ particles were clearly segregated. Upon observing the yellowish hue of the solution fade and become clear, the solvent was extracted with a syringe and used for Raman spectroscopy. XRD measurements were performed using a D8 Advance Bruker powder x-ray diffractometer with Cu K_α radiation (1.540 60 Å), K_{α1} (1.540 60 Å), K_{α2} (1.544 43 Å) and K_β (1.392 22 Å). Electrophoretically separated nanoparticles from crystalline sols at different pH levels were vacuum dried at low temperature (90 °C) in an electric furnace to evaporate the solvent and its by-products. The remaining powders were collected for XRD analysis. The XRD data analysis was performed using X'Pert HighScore Plus PANalytical software. The morphology of the PC substrate before and after TiO₂ thin film deposition was studied with tapping mode AFM (Digital Instruments) in air. NANOSENSORS SuperSharpSilicon probes with a typical tip radius of 2 nm, a spring force constant of 1.3 N m⁻¹, and a resonant frequency of ~61 kHz were employed in the measurements. The photocatalytic activity was evaluated by monitoring the degradation of 5 μM MB solution under UV illumination using a UV lamp (SPECTROLINE BLE-5T254 5 W, main spectral peak: 254 nm). The samples were placed horizontally within a beaker containing a 10 ml aqueous MB solution under constant stirring. The beaker was kept encased in an enclosure with the UV lamp installed inside. Initially, the samples were kept submerged in the MB solution in the dark for 75 min. The samples were then irradiated from above for a period of

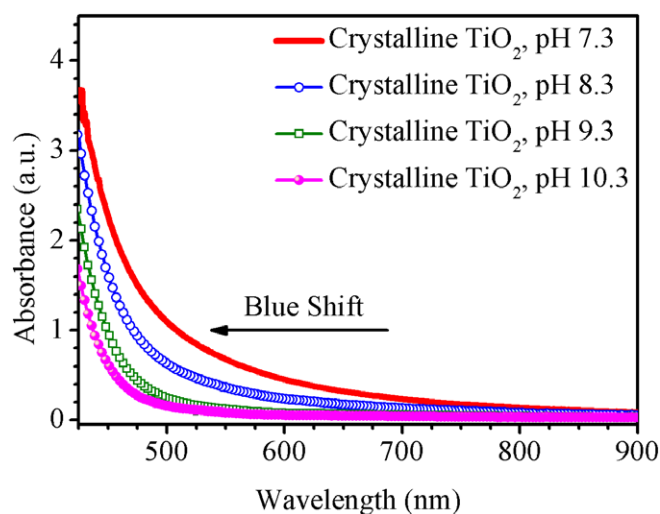


Figure 1. UV–Vis optical absorption spectra of the prepared 1 wt% crystalline TiO₂ suspended in water at different pH levels ranging from 7.3 to 10.3.

150 min. The intensity of the absorption peak at 663 nm was measured using UV–Vis spectrophotometry at 10 min intervals to probe the degradation process.

3. Results and discussion

3.1. Optical properties study

The spectral optical absorption measurements are used to study the optical properties of the prepared crystalline TiO₂ sol and the thin films. Figure 1 presents the UV–Vis absorption spectra of the prepared 1 wt% crystalline TiO₂ in water at different pH levels ranging from 7.3 to 10.3 (7.3, 8.3, 9.3, and 10.3), in a quartz cuvette of 10 mm path length. The spectra depict that the minima of the spectral absorption for all studied solutions are in the visible region. Increasing the pH shifts the TiO₂ absorption cut-off—i.e. where the absorbance value is nearly minimal—towards shorter wavelengths (blue shift). The observed blue shift could partially be due to the different particle and crystallite sizes.

The optical indirect bandgap energy (E_g) of the crystalline TiO₂ colloidal solutions at different pH levels can be calculated according to equation (1) [35],

$$\alpha h\nu = A(h\nu - E_g)^m, \quad (1)$$

where A is a constant which depends on the type of the semiconductor, h is the Planck constant (4.1357×10^{-15} eV s), ν is the frequency, α is the absorption coefficient, and m is equal to 0.5 and 2 for direct and indirect transitions, respectively. Since TiO₂ is an indirect transition semiconductor, extrapolating the straight line portion of $(\alpha h\nu)^{0.5}$ versus $h\nu$ graph to the abscissa yields the indirect bandgap of different TiO₂ samples, as shown in figure 2(a). The optical indirect bandgaps of the crystalline TiO₂ solutions were calculated as 2.35 eV, 2.42 eV, 2.55 eV and 2.60 eV at pH 7.3, 8.3, 9.3 and 10.3, respectively (figure 2(a)). It is essential to note that the optical indirect bandgap is different than the

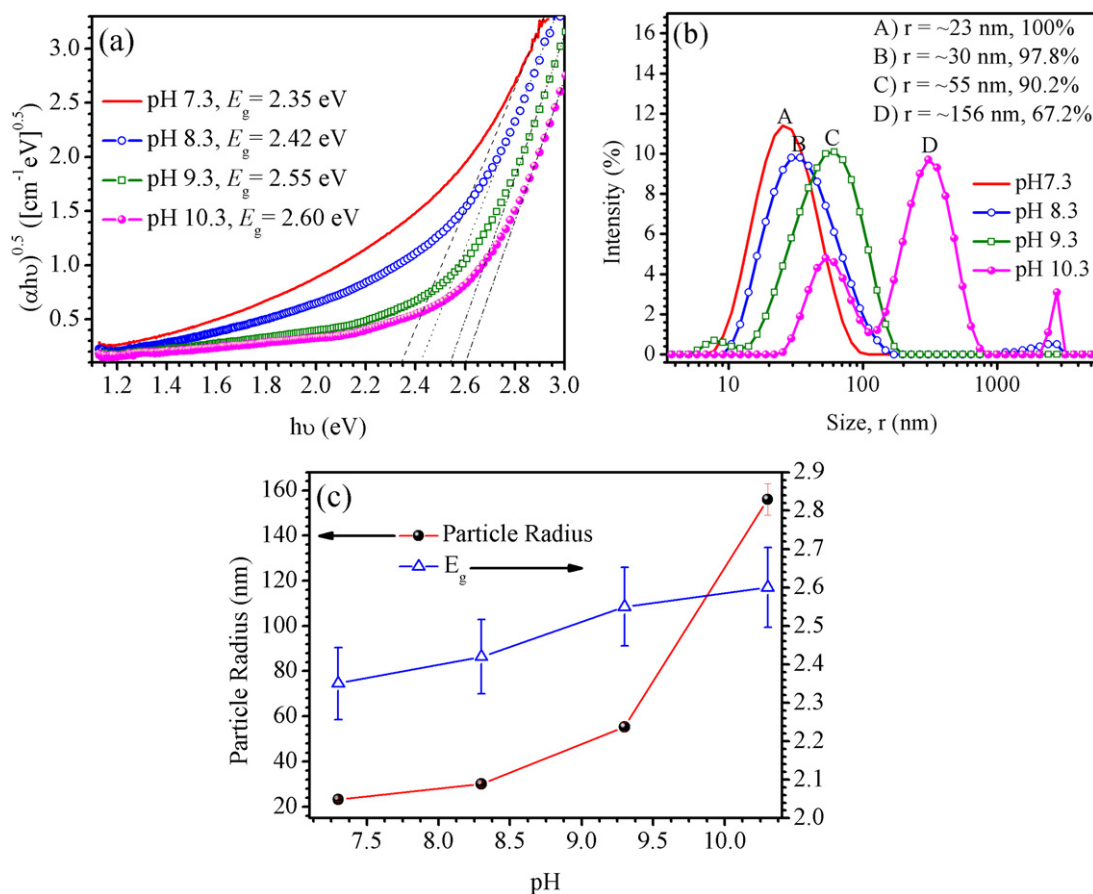


Figure 2. (a) Plot of the indirect transition of the nanocrystalline TiO₂ at different pH levels (7.3, 8.3, 9.3 and 10.3). The dash, dot, dashed–dotted, and dashed–dotted–dotted lines within the bandgap absorption region are shown to determine the indirect bandgap energies, (b) distribution of hydrodynamic radii for TiO₂ nanoparticles at different pH levels derived from DLS measurements and (c) the variation of average particle radius and optical indirect bandgap with changes in pH. The percentages (%) in (b) show what portion of the solution has the stated nanoparticle size.

electronic bandgap. The interestingly low observed optical indirect bandgap energies of the crystalline TiO₂ colloidal solutions here, call for additional research to measure the electronic bandgap by x-ray photoemission spectroscopy as well as surface imaging by a scanning tunnelling microscope (STM) to clarify the effect of surface states or defects and lattice imperfections, respectively. Recently, it was shown that the surface states of a two-dimensional phase of TiO₂ might have a lower bandgap compared to the bulk TiO₂ [36, 37]. This difference might be related either to surface-state-induced band bending [36], Ti interstitial species in the TiO₂ bulk that can diffuse to the surface in the presence of oxygen and form a new TiO₂ phase with lower bandgap [37], or to surface defects. In particular, the density of surface states is intrinsically high in nanoparticles. Our preliminary results (unpublished data) show that the surface states of the synthesized TiO₂ particles have a significant effect on its relatively low bandgap. A detailed study on electronic band structure of the synthesized samples is underway in our laboratory and will be reported in forthcoming papers.

The distinct linear pattern in this plot denotes the onset of absorption. In general, the morphology and the self-cleaning properties of the resultant TiO₂ films can be partially affected

by the secondary particle distribution. Hence, it is important to control the particle size and agglomerate distribution of the colloids. In this study, the relationship between TiO₂ nanoparticle hydrodynamic radius (r) and pH was studied experimentally using DLS. The size measured using DLS includes the shear layer around the nanoparticles, i.e., it over-estimates the size by a few nanometres [9]. Figure 2(b) shows that by changing the pH of the peroxotitanium complexes, size-controllable TiO₂ nanoparticles may be produced. The average radius of the TiO₂ nanoparticles increasing with increasing pH levels of the reaction mixture. The estimated radii for the main peaks in figure 2(b) correspond to about 23 nm, 30 nm, 55 nm and 156 nm at pH 7.3, 8.3, 9.3 and 10.3, respectively. The water-soluble crystalline colloidal solutions, obtained at pH 7.3 and 8.3, were stable for more than one year. The as-obtained precipitates—i.e. the crystalline TiO₂ nanoparticles after isolation from solvent by electrophoresis—were capable of being re-dispersed in water to re-form stable colloidal solution. The state of the art for preparation of soluble TiO₂ nanoparticles makes use of organic modifiers and surfactants to tailor the particles' surface properties. This eventually leads to diminished solubility, which is a result of modifier/surfactant molecules that cannot be removed [38]. Recently, Zhao *et al* also have

successfully synthesized surfactant-free water-soluble anatase nanoparticles based on the hydrolysis and condensation of tetramethoxysilane (TMOS) [38].

It was observed that by increasing the pH, the monodisperse TiO₂ colloidal solutions at pH 7.3 give away to polydisperse solutions at higher pH levels that suggest the onset of precipitation (figure 2(b)). The size of crystalline TiO₂ particles is strongly dependent on the acidity of the peroxotitanium complex. The electrostatic surface charge of TiO₂ particles and its surface chemical composition may be altered by varying the density of hydroxyl groups. A lower surface acidity of TiO₂ nanoparticles—i.e. higher concentrations of hydroxyl groups—demote the rate of hydrolysis reactions which leads to formation of aggregates. Higher pH likely facilitates the mutual contact of surface hydroxyl groups between particles, leading to the strong inter-linkage of TiO₂ particles [38]. It was observed that nanoparticle solutions prepared at pH 10.3 were only stable for 10 days, after which the TiO₂ solution transformed from an aqueous form to a gel. In a basic environment, there exist strong attractive effects due to the negative surface charges of the titanium clusters [39].

Figure 2(a) demonstrates that the indirect bandgap energies of the crystalline TiO₂ colloidal solutions prepared at lower pH levels are narrower than those prepared at higher levels. In the structures with relatively small grain size (<100 nm), the bandgap widening (blue shift in the absorption edge) is generally expected with reduction in the particle size (quantum confinement effects) [40]. Herein a wider bandgap was observed in the sample with larger particle size. This suggests that in this case the optical indirect bandgap energy is mainly under the influence of chemical composition/phase crystallinity rather than the particle size since the TiO₂ nanoparticles surface composition—i.e. the crystallinity and the density of the surface hydroxyl groups—does not remain constant by changing the pH of the peroxotitanium complex (or as the prevalence of either the anatase or rutile phase varies). This is elaborated on in the ‘structural properties study’ section. Anatase and rutile (two forms of TiO₂) are different in mass density and electronic band structure due to disparities in lattice structures [4]. Furthermore, because the crystallinity of the anatase phase degrades with an increase in the density of hydroxyl groups residing on the particles’ surface, the predominance of an amorphous phase increases (structural properties study section—Raman and XRD analysis), where a considerable blue shift in the absorption edge is observed. As a result of an increase in the amorphous content, the grain boundaries and imperfections decrease. This leads to larger free carrier concentrations and the existence of potential barriers [41]. The electric fields arising from these factors result in an increase in the optical bandgap, as explained elsewhere [41].

As mentioned earlier in this work, the treated PC substrates were spin-coated with the synthesized TiO₂ sols at different pH levels. A pre-coat of peroxotitanium complex was employed initially to protect the substrate from photocatalytic degradation and also to provide improved adhesion. Figure 3 displays typical transmittance spectra for the coated substrates.

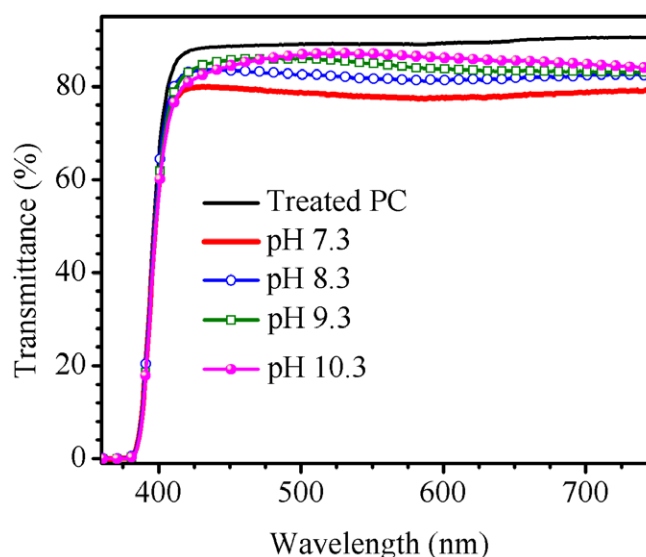


Figure 3. UV-Vis transmission spectra of the coated substrates at different pH levels.

One observes that the transmittance of the samples in the visible region (400–700 nm) decreased due to the high refractive index of TiO₂, which causes high reflectivity. The refractive index for TiO₂ layers on PC has been previously estimated at about 2.0 [9]. The thickness of the applied thin films, from the sol prepared at pH 7.3, was calculated to be ~105 nm. The method of thickness measurement has been explained in detail elsewhere [9, 42]. This thin film includes four crystalline layers along with an amorphous pre-coat layer.

3.2. Structural properties study

3.2.1. Raman spectroscopy. Herein, Raman spectroscopy was applied to probe the effect of TiO₂ surface hydroxyl groups on the phase/structural transformation. The previous efforts include the non-stoichiometry effects for TiO₂ nanocrystals obtained at 100–650 °C [27], and the phase transformation of TiO₂ from anatase to rutile in the range of 200–800 °C by UV and visible Raman spectroscopy [43]. A previous study has also analysed the stress and strain of anatase TiO₂ films with Raman spectroscopy [44]. Additionally, Swamy *et al* have studied the size-dependent modifications of the Raman spectrum of rutile TiO₂ [45]. In the current study, Raman spectroscopic investigations of phonons of different symmetries in TiO₂ nanocrystals synthesized by the sol-gel method were carried out. Figure 4(a) shows Raman spectra of crystalline TiO₂ solutions with different pH conditions. To verify that the appearance of the bands is caused by TiO₂ nanoparticles and not the solvent (water), the nanoparticles were isolated with the previously mentioned electrophoresis technique. There are a total of six Raman bands which are absent in the spectra of the aqueous solution without the presence of TiO₂ nanoparticles (figure 4(b)).

Figure 4(a) indicates five major bands at ~150, 285, ~508, 678 and 906 cm⁻¹ and another weak band at 822 cm⁻¹. Two Raman bands of the anatase phase of TiO₂ were observed at ~150 and ~508 cm⁻¹. These bands are assigned to E_g

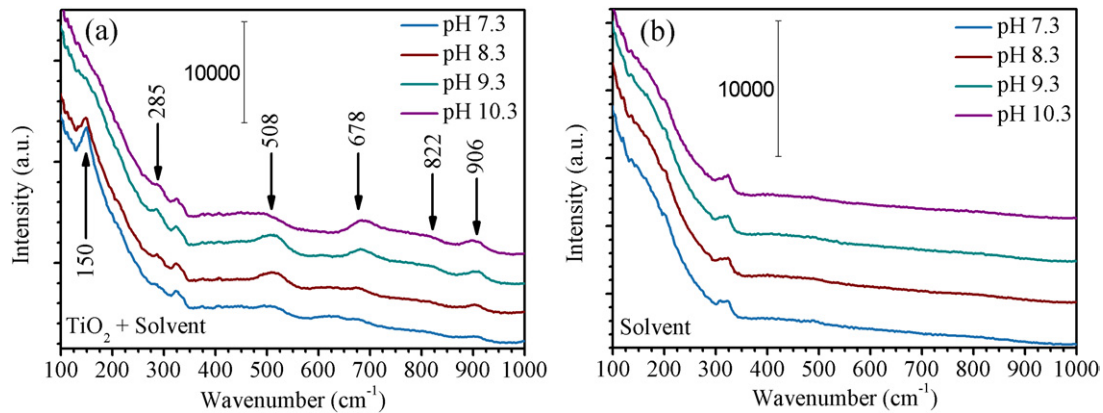


Figure 4. (a) Raman spectra of the crystalline TiO_2 solutions with different pH levels (pH 7.3: turquoise colour, pH 8.3: wine colour, pH 9.3: light green colour and pH 10.3: violet colour). (b) Raman spectra of the isolated solvents with different pH levels following the separation of TiO_2 nanoparticles using the electrophoresis technique.

and B_{1g}/A_{1g} photonic modes, respectively [43, 46]. The E_g mode centred around 150 cm^{-1} is the most commonly used anatase Raman band to probe phonon confinement effects [47]. One can see from figure 4(a) that a change in the pH of the peroxotitanium complex from 7.3 to 8.3 induces a shift (towards lower wavenumbers) of the $\sim 150\text{ cm}^{-1}$ E_g phonon mode for crystalline nanoparticles of larger sizes (see the online supporting information for figure scaled to emphasize the area of interest (stacks.iop.org/JPhysD/46/505316/mmedia)). This is in line with the above DLS observations which showed larger particles sizes for the pH 8.3 versus pH 7.3 samples. As can be seen, Raman active phonons of rutile at 442 cm^{-1} (E_g), 607 cm^{-1} (A_{1g}) and 692 cm^{-1} are absent in the presented Raman spectra in figure 4(a) [48]. Conversely, further structural analysis by XRD later shows the presence of rutile peaks in the pattern. One notes that the appearance of rutile peaks in XRD patterns is most likely due to the post-annealing of the crystalline TiO_2 nanoparticles at 90°C , which give rise to the formation of rutile. The Raman band at 668 cm^{-1} could be interpreted as Ti–O–Ti crystal phonons [48–50], which is shifted to 678 cm^{-1} in the presented Raman spectra (figure 4(a)). Several factors including a heterogeneous size distribution [51, 52], as well as defects and non-stoichiometry may contribute to the changes in the peak position, line-width, and the shape of the Raman modes [53]. It was demonstrated that the Raman lines become also weak and broad when the samples have local lattice imperfections that might be related to the oxygen stoichiometry of the material and crystallinity [27, 53]. Hence, absence of the observed strong peak at 150 cm^{-1} at pH 9.3 and 10.3 as well as the change in the line-width and the shape of Raman band at 678 cm^{-1} , can be described by the increase in the amount of the noncrystalline phase (defects or more amorphous content) as well as increase in the heterogeneity of the size distribution (confirmed by the broadening of the particle size distributions obtained from DLS). This is elaborated on in XRD section in this paper. The weak band at 822 cm^{-1} is related to a covalent Ti–O–H bond [46, 49], while the vibration band at 906 cm^{-1} could also be attributed to Ti–O–H bonds [49]. It has already been shown for TiO_2 nanotubes that the Raman band at 922 cm^{-1} is related to Ti–O–H vibrations [49, 50]. In this study, the pH effect of the peroxotitanium complex

on the structure of crystalline TiO_2 was mainly shown in the intensity increase of the band at 906 cm^{-1} . The pH alerts on the protonation and de-protonation equilibrium of surface hydroxylated groups. The use of NH_4OH to adjust the pH levels of the samples can promote the formation of Ti–O–H. As pH increases during the refluxing process, TiO_2 can preferably bind to the –OH– groups surrounding the crystalline phase which results in interrupting the formation of the anatase. The increase in pH gradually enhances the peak at 906 cm^{-1} , while simultaneously causing the strong peak at 150 cm^{-1} to fade away. By increasing the pH of the peroxotitanium complex the intensity of the weak band at 822 cm^{-1} (covalent Ti–O–H) increases slightly, as well. The Raman bands at 285 and 678 cm^{-1} have been previously observed for the TiO_2 anatase dried at 373 K [49]. High temperatures can induce the transform of the TiO_2 structure [49]. Hence, the presence of the Raman peaks at 285 and 678 cm^{-1} suggest that a higher pH environment (in the peroxotitanium complex) might play the same role as high-temperature annealing in the structural transformation of crystalline TiO_2 . The above-mentioned Raman study regarding the TiO_2 amorphous samples treated with different pH levels indicates that the pH environment affects the formation of the anatase phase of TiO_2 . It can be deduced that, as the pH level increases, the formation of the anatase phase of TiO_2 is inhibited, which leads to the transformation of the TiO_2 structures.

3.2.2. X-ray diffraction. The effect of pH on the average crystallite size and crystallinity was studied by XRD. Figure 5(a) shows the XRD patterns of the TiO_2 particles obtained from the sols synthesized at different pH levels (7.3, 8.3, 9.3 and 10.3). The relative intensity of the diffraction lines indicates that the crystallinity of TiO_2 nanoparticles is closely related with the concentration of –OH– groups on the TiO_2 surface in the peroxotitanium complex. The intense diffraction lines at (1 1 0) and (1 0 1) for vacuum dried sols prepared from peroxotitanium complexes at pH levels 7.3 and 8.3, indicate high levels of crystallinity. This is in contrast to the patterns of dried TiO_2 nanoparticles at pH 9.3–10.3, which exhibit broad (1 1 0) and (1 0 1) peaks

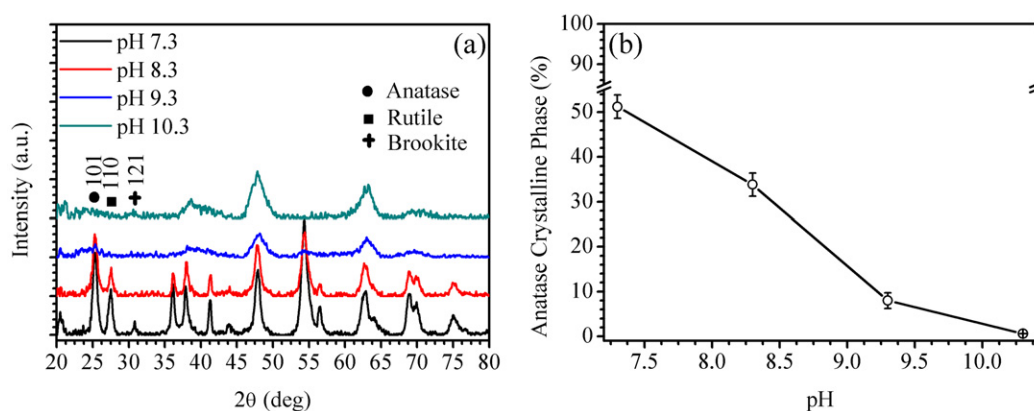


Figure 5. (a) XRD patterns of dried TiO₂ crystalline particles prepared from solutions at different pH (7.3 to 10.3) annealed at 90 °C and (b) the share of anatase crystalline phase versus pH. (1 0 1), (1 1 0) and (1 2 1) show 100% intensity XRD peaks for anatase, rutile and brookite, respectively. The intensity of the main anatase, rutile, and brookite peaks decreases with increase in pH.

indicating inferior crystallinity. The decrease in the intensity of the main XRD peaks—i.e. (1 0 1), (1 1 0) and (1 2 1)—with increases in pH could partially be attributed to processes such as coarsening and aggregation–recrystallization and/or to inferior crystallinity. The calculation of the crystalline share was performed automatically on software using the Rietveld refinement. The main contribution for the anatase, rutile, and brookite shares comes from the major 100% intensity peaks at (1 0 1), (1 1 0), (1 2 1), respectively. For pH 7.3 and 8.3, anatase was the predominant crystalline phase (figure 5(a)).

The average crystallite size of the anatase phase was calculated using the Debye-Scherrer's formula from the full-width at half-maximum (FWHM) of the (1 0 1) reflection—i.e. the most intense diffraction peak—for anatase [13]:

$$D = \frac{0.9\lambda}{B \cos \theta}, \quad B = \sqrt{B_m^2 - B_s^2}, \quad (2)$$

where D is the crystallite size, λ is the x-ray radiation wavelength (0.154 060 nm); B_m and B_s are the reflection FWHM of the measured sample and the standard sample, respectively. A detailed analysis of figure 5(a) demonstrates that for the 100% intensity (1 0 1) peak of anatase, the FWHM decreases to a small degree from ~ 0.76 to ~ 0.69 with pH increasing from 7.3 to 8.3. This indicates a small increase in the crystallite size. The estimated average anatase crystallite size increased from ~ 10.7 to ~ 11.8 nm by increasing the pH of the peroxotitanium complex from 7.3 to 8.3, respectively. The size of particle which can be quantified by DLS technique is essentially different from the crystallite size, which can be estimated from XRD data. The comparison between this observation and DLS analysis evidently demonstrates that each particle has a polycrystalline nature. It can be concluded from figure 5(b) that the calculated anatase phase content decreased as the pH of the amorphous solution increased from 7.3 to 10.3. Increasing the pH of the amorphous complex to levels > 8.3 , resulted in a noticeable transition in crystallinity from long-range order to short-range order, suggesting that higher densities of hydroxyl groups leads to inferior crystal quality. This can be confirmed by the observation of the significant reduction in the intensity of (1 0 1) and (1 1 0) reflections, which is consistent with the Raman spectroscopy results. The

XRD peaks located at $\sim 48^\circ$ and $\sim 62.7^\circ$ are caused by the overlap of several phases. Although the share of anatase crystalline phase decreases as the pH increases from 7.3 to 10.3, the increase in the intensity of these peaks to a small degree at pH 10.3 is likely due to the presence of more brookite TiO₂.

The kinetics of phase transformations in TiO₂ has been already extensively reviewed [54]. It is commonly accepted that high-temperature annealing, at least 610 to 695 °C, is required for anatase to rutile transformation, while the transformation becomes immeasurably slow below the mentioned temperature range. However, the rutile particles obtained via high-temperature calcination of anatase phase are agglomerated due to growth of the nanocrystalline particles [55]. We have previously developed thin films of fully anatase TiO₂ on PC from peroxotitanium complexes refluxed at pH 7, which showed all reflections correspond to the anatase phase (see the online supporting information for XRD pattern of colloids obtained at pH 7 (stacks.iop.org/JPhysD/46/505316/mmedia)) [9, 13]. The comparison between XRD analysis in the current study and our previous works [9, 13], shows that increasing the pH of the peroxotitanium complex coupled with low-temperature annealing (90 °C) can be considered as a simple and inexpensive way to prepare active phase-mixed rutile-anatase photocatalysts for wet coating applications at low temperatures. This is also in line with the observations in Raman section in this paper, which showed that increasing the pH of the peroxotitanium complex impedes the formation of anatase phase. In good agreement with the Raman spectroscopy results, the XRD analysis simply shows that for pH 10.3, a substantial part of the solid was not crystallized. Our earlier investigation on XRD patterns of TiO₂ thin films annealed at various temperatures (100–500 °C) demonstrated that annealing at elevated temperatures does not induce anatase to rutile transformation [13].

3.3. Morphological properties study

The surface morphology of the TiO₂ films deposited on PC substrates is investigated by AFM operating in tapping mode.

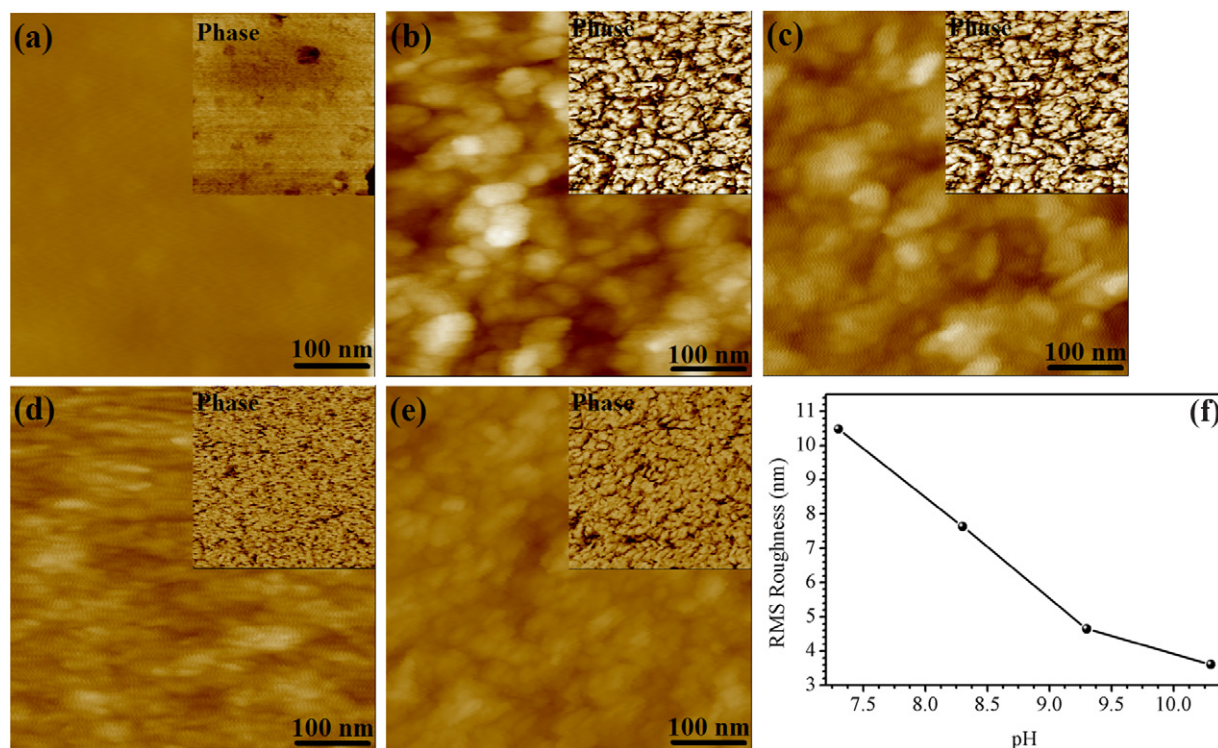


Figure 6. AFM micrographs of (a) PC and TiO₂ films prepared on PC substrate with a layer of amorphous pre-coat and four crystalline layers from (b) pH 7.3 (anatase phase content: 51.2%), (c) pH 8.3 (anatase phase content: 33.8%), (d) pH 9.3 (anatase phase content: 8%) and (e) pH 10.3 (anatase phase content: 0.6%). (f) RMS roughness of layers. The insets (a)–(e) depict the relevant phase images.

The AFM (scan area 500 nm × 500 nm) micrographs of a PC substrate before and after deposition of TiO₂ crystalline layers, applied from refluxed peroxotitanium complexes at different pH levels, are shown in two-dimensions (2D) in figure 6. The phase images (insets) of the developed crystalline TiO₂ with varying pH show uniform layers on the PC surface. The AFM micrographs confirm the decrease in the anatase crystalline phase share with an increase in pH. This can be observed in the relatively rough granular morphology of anatase in figures 6(b) and (c) (RMS roughnesses of ~10.5 nm and ~7.5 nm, respectively), which is shown to change gradually as the intensity of –OH– groups on the TiO₂ particles increases in figures 6(d) and (e) (RMS roughnesses of ~4.6 nm and ~3.6 nm, respectively).

The interpretation of the AFM results in terms of surface morphology agrees with the observation of the reduction in the anatase (1 0 1) reflection (figure 5(a)) with increases in pH. This can be attributed to the reduction in the prevalence of the anatase crystalline phase with respect to other TiO₂ phases (figure 4(b)) which led to a decrease in RMS roughness of the surfaces. Additionally, it can be noted that the roughness is caused by the granular structure, which also results in a high surface area. Hence, it is expected that crystalline layers prepared from the complex at pH 7.3, exhibit higher self-cleaning activity compared to other samples. This is partially due to the fact that this layer has the highest RMS roughness.

3.4. Self-cleaning properties study

Degradation of MB was used as a measure of the photocatalytic activity of the films. Figure 7(a) shows the absorbance spectra

of the MB solution at different UV illumination times for the thin films applied on PC from the pH 7.3 sol.

The peak intensity at 663 nm was used to estimate the relative concentration of MB in the solution. Increasing the illumination time leads to decreased MB concentration. The relative concentration of MB as a function of illumination time is displayed in figure 7(b). The pH 7.3 sample, with a total degradation of ~77%, shows the highest self-cleaning activity. Similar degradation was observed for dip-coated thin films with comparable thickness of pure anatase on PC in our previous work [9]. It is important to note that the UV lamp used in the previous work had two emission lines; a major emission line at 254 nm and second weaker one at 365 nm. The lamp used in this study has only one emission line, which is at 254 nm, i.e. less UV radiation is emitted.

There are several reasons that may account for the higher self-cleaning activities of the films prepared from lower pH levels in this study. First, higher levels of crystallinity at lower pH levels (i.e. 7.3 and 8.3), shown in figures 5(a) and (b), plays an important role in the enhancement of the self-cleaning activities. Second, smaller anatase crystallite sizes could shorten the route for an electron as it migrates from the conduction band of the anatase TiO₂ to its surface. Additionally, smaller particle size also accounts for a higher surface area. As mentioned before, the roughness is caused by the granular structure, which also provides a high surface area. Hence, it is expected that crystalline layers prepared from the complexes at pH 7.3 and 8.3—with RMS roughnesses of ~10.5 and 7.5 nm, respectively—exhibit higher photocatalytic activity compared to other samples.

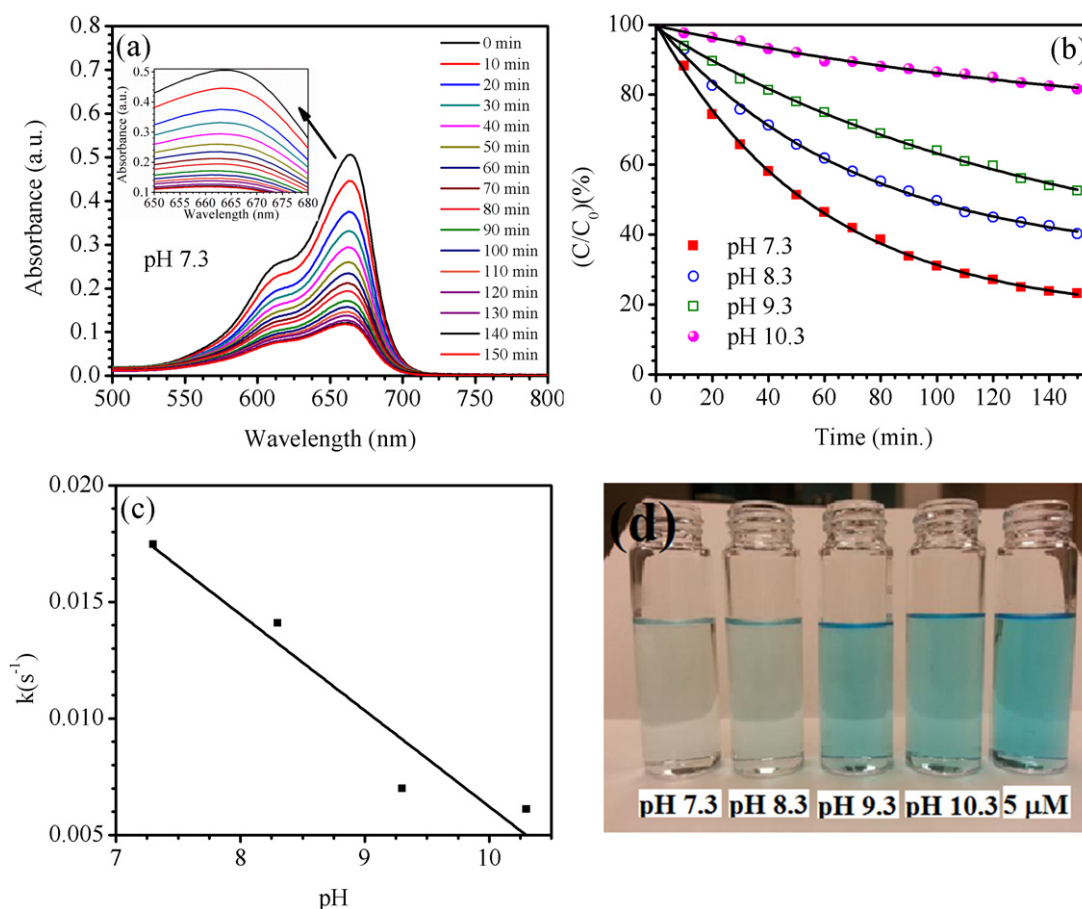


Figure 7. (a) The absorbance spectra of MB solution under UV illumination for the pH 7.3 sample, (b) (C/C_0) (%) versus illumination time for different samples. (c) Photocatalytic reaction rate constants (k) versus the pH. (d) A picture of the original $5 \mu\text{M}$ MB solution before and after the photocatalytic tests.

Therefore, poor crystallinity is most likely the primary reason for the low photocatalytic activity of thin films prepared from the complexes synthesized at higher pH levels (i.e. 9.3 and 10.3). For the TiO_2 thin films prepared from the sol at pH 10.3, the MB degradation is negligible, i.e. very minute photocatalytic activity is observed. This is consistent with our observations of the crystallinity of TiO_2 nanoparticles at each pH level described in the XRD section. The rate of degradation also is higher for the films prepared at lower pH levels, that is, the smaller nanoparticles with lower density of $-\text{OH}-$ groups on the surface along with a greater portion of the anatase phase show higher photocatalytic activity. The degradation curves in figure 7(b) are, to a good approximation, exponential decay curves. Therefore, the photocatalytic reaction is a first-order reaction with a reaction rate constant k , where $C/C_0 = \exp(-kt)$. The values of k for samples with different pH levels are shown in figure 7(c). It is observed that k decreases linearly with increasing the pH levels of the peroxotitanium complex.

4. Conclusion

It was shown that active phase-mixed anatase-rutile photocatalysts for wet coating applications can be prepared from peroxotitanium complexes at pH 7.3–8.3 with low-temperature annealing. As a whole, the crystallinity of

the anatase phase degrades with an increase in the density of hydroxyl groups residing on the particles' surface and the predominance of the amorphous phase increases with pH, as well. The anatase phase contents were shown to be 51.2%, 33.8%, 8% and 0.6% for samples at pH 7.3, 8.3, 9.3 and 10.3, respectively. It was observed that by increasing the pH, the monodispersity of the TiO_2 colloidal solution at pH 7.3 gives away to polydispersity as higher pH levels show mixtures of nanoparticles of different diameters. Higher pH of the peroxotitanium complex likely facilitates the mutual contact of surface hydroxyl groups between crystalline particles, leading to the strong inter-linkage of crystalline TiO_2 particles and larger average particle size. Increasing the pH causes a blue shift in the TiO_2 absorption cut-off and a widening of the optical indirect bandgap of the crystalline TiO_2 from 2.35 eV for pH 7.3 to 2.60 eV for pH 10.3. Thin films prepared at lower pH showed more defined granular morphology and higher RMS roughness. Better self-cleaning activity was observed for films prepared at lower pH levels.

Acknowledgments

The authors would like to thank R Tufts, assistant director of Nanotechnology Research and Education Center (NREC) at the University of South Florida (USF) and N Shanahan at

civil engineering department (USF) for valuable discussions on XRD analysis. We would like to thank C Eaton for valuable help editing the manuscript.

References

- [1] Fujishima A and Honda K 1972 *Nature* **238** 37–8
- [2] Fujishima A, Rao T N and Tryk D A 2000 *J. Photochem. Photobiol. C* **1** 1–21
- [3] Hagfeldt A and Graetzel M 1995 *Chem. Rev.* **95** 49–68
- [4] Linsebigler A L, Lu G and Yates J T 1995 *Chem. Rev.* **95** 735–58
- [5] Yaghoubi H 2013 Self-cleaning materials for plastic and plastic-containing substrates *Self-Cleaning Materials and Surfaces: a Nanotechnology Approach* ed W A Daoud (Chichester: Wiley) pp 153–202
- [6] Fujishima A, Zhang X and Tryk D A 2008 *Surf. Sci. Rep.* **63** 515–82
- [7] Fujishima A and Zhang X 2006 *C. R. Chim.* **9** 750–60
- [8] Fujishima A, Nakata K, Ochiai T, Manivannan A and Tryk D A 2013 *Electrochem. Soc. Interface* **22** 51–6
- [9] Yaghoubi H, Taghavinia N and Alamdari E K 2010 *Surf. Coat. Technol.* **204** 1562–1568
- [10] Nakata K and Fujishima A 2012 *J. Photochem. Photobiol. C* **13** 169–189
- [11] Nakata K, Ochiai T, Murakami T and Fujishima A 2012 *Electrochim. Acta* **84** 103–111
- [12] Ganesh V A, Raut H K, Nair A S and Ramakrishna S 2011 *J. Mater. Chem.* **21** 16304–16322
- [13] Yaghoubi H, Taghavinia N, Alamdari E K and Volinsky A A 2010 *ACS Appl. Mater. Interfaces* **2** 2629–36
- [14] Feng R et al 2013 *Nanotechnology* **24** 255603–12
- [15] Chen J and Poon C-s 2009 *Build. Environ.* **44** 1899–1906
- [16] Ohama Y and Van Gemert D 2011 Application of Titanium Dioxide Photocatalysis to Construction Materials: State-of-the-Art Report of the RILEM Technical Committee 194-TDP (RILEM State-of-the-Art Reports), vol. 5 (London/New York: Springer)
- [17] Wu D and Long M 2011 *ACS Appl. Mater. Interfaces* **3** 4770–4
- [18] Afzal S, Daoud W A and Langford S J 2012 *J. Mater. Chem.* **22** 4083–8
- [19] Tung W S and Daoud W A 2011 *J. Mater. Chem.* **21** 7858–69
- [20] Qi K, Daoud W A, Xin J H, Mak C L, Tang W and Cheung W P 2006 *J. Mater. Chem.* **16** 4567–74
- [21] Lee J A, Krogman K C, Ma M, Hill R M, Hammond P T and Rutledge G C 2009 *Adv. Mater.* **21** 1252–6
- [22] Baghriche O, Rtimi S, Pulgarin C, Roussel C and Kiwi J 2013 *Appl. Catal. B* **130–131** 65–72
- [23] Lee C-S, Kim J, Son J Y, Choi W and Kim H 2009 *Appl. Catal. B* **91** 628–33
- [24] Carneiro J O, Teixeira V, Portinha A, Magalhães A, Coutinho P, Tavares C J and Newton R 2007 *Mater. Sci. Eng. B* **138** 144–50
- [25] Hu Y and Yuan C 2006 *J. Mater. Sci. Technol.* **22** 239–44
- [26] Oosawa Y and Gratzel M 1984 *J. Chem. Soc., Chem. Commun.* **24** 1629–30
- [27] Zhang W F, He Y L, Zhang M S, Yin Z and Chen Q 2000 *J. Phys. D: Appl. Phys.* **33** 912–16
- [28] Bersani D, Lottici P P and Ding X-Z 1998 *Appl. Phys. Lett.* **72** 73–75
- [29] Balaji S, Djaoued Y and Robichaud J 2006 *J. Raman Spectrosc.* **37** 1416–22
- [30] Sahoo S, Arora A K and Sridharan V 2009 *J. Phys. Chem. C* **113** 16927–33
- [31] Batzill M 2011 *Energy Environ. Sci.* **4** 3275–86
- [32] Hosseingholi M, Pazouki M, Hosseinnia A and Aboutaleb S H 2011 *J. Phys. D: Appl. Phys.* **44** 055402
- [33] Pottier A, Cassaignon S, Chaneac C, Villain F, Tronc E and Jolivet J-P 2003 *J. Mater. Chem.* **13** 877–82
- [34] Simonsen M E, Li Z and Søgaaard E G 2009 *Appl. Surf. Sci.* **255** 8054–62
- [35] Dakhel A A 2009 *Opt. Mater.* **31** 691–695
- [36] Zhang Z and Yates J T 2012 *Chem. Rev.* **112** 5520–51
- [37] Tao J, Luttrell T and Batzill M 2011 *Nature Chem.* **3** 296–300
- [38] Zhao Y, Ren W and Cui H 2013 *J. Colloid Interface Sci.* **398** 7–12
- [39] Simonsen M E and Søgaaard E G 2010 *J. Sol–Gel Sci. Technol.* **53** 485–497
- [40] Wolkin M V, Jorne J, Fauchet P M, Allan G and Delerue C 1999 *Phys. Rev. Lett.* **82** 197–200
- [41] Ramana C V, Smith R J and Hussain O M 2003 *Phys. Status Solidi a* **199** R4–6
- [42] Taghavinia N and Yao T 2004 *Physica E* **21** 96–102
- [43] Zhang J, Li M, Feng Z, Chen J and Li C 2005 *J. Phys. Chem. B* **110** 927–35
- [44] Alhomoudi I A and Newaz G 2009 *Thin Solid Films* **517** 4372–8
- [45] Swamy V, Muddle B C and Dai Q 2006 *Appl. Phys. Lett.* **89** 163118–3
- [46] Qian L, Du Z-L, Yang S-Y and Jin Z-S 2005 *J. Mol. Struct.* **749** 103–7
- [47] Han C, Pelaez M, Likodimos V, Kontos A G, Falaras P, O’Shea K and Dionysiou D D 2011 *Appl. Catal. B* **107** 77–87
- [48] Bavykin D V, Friedrich J M, Lapkin A A and Walsh F C 2006 *Chem. Mater.* **18** 1124–1129
- [49] Rendón-Rivera A, Toledo-Antonio J A, Cortés-Jácome M A and Angeles-Chávez C 2011 *Catal. Today* **166** 18–24
- [50] Cortés-Jácome M A, Ferrat-Torres G, Ortiz L F F, Angeles-Chávez C, López-Salinas E, Escobar J, Mosqueira M L and Toledo-Antonio J A 2007 *Catal. Today* **126** 248–255
- [51] Šćepanović M J, Grujić-Brojčin M, Dohčević-Mitrović Z D and Popović Z V 2007 *Appl. Phys. A* **86** 365–371
- [52] Spanier J E, Robinson R D, Zhang F, Chan S-W and Herman I P 2001 *Phys. Rev. B* **64** 245407
- [53] Parker J C and Siegel R W 1990 *Appl. Phys. Lett.* **57** 943–5
- [54] Zhang H and Banfield J F 2000 *J. Phys. Chem. B* **104** 3481–7
- [55] Wu M, Lin G, Chen D, Wang G, He D, Feng S and Xu R 2002 *Chem. Mater.* **14** 1974–80